Spectroscopic and Dynamic Properties of the Peridinin Lowest Singlet Excited States†

Donatas Zigmantas,‡ Tomáš Polívka,‡ Roger G. Hiller,§ Arkady Yartsev,‡ and Villy Sundström*,‡

Department of Chemical Physics, Lund University, Box 124, S-22100 Lund, Sweden, and Department of Biological Sciences, Macquarie University, NSW, Australia 2109

Received: January 4, 2001; In Final Form: April 4, 2001

Spectroscopic properties as well as excited state dynamics of the carotenoid peridinin in several solvents of different polarities were investigated by time-resolved fluorescence and transient absorption techniques. A strong dependence of the peridinin lowest excited states dynamics on solvent polarity was observed after excitation into the strongly allowed S_2 state. Peridinin relaxes to the ground state within 10 ps in the strongly polar solvent methanol, while in the nonpolar solvent *n*-hexane a 160 ps lifetime was observed, thus confirming the previous observations revealed by transient absorption spectroscopy in the visible region (Bautista, J. A.; et al. *J. Phys. Chem. B* **1999**, *103*, 8751). In addition, the solvent dependence in the near-IR region is demonstrated by a strong negative feature in the transient absorption spectrum of peridinin in methanol, which is not present in *n*-hexane. This band, characterized by a 1 ps rise time, is ascribed to stimulated emission from an intramolecular charge-transfer (ICT) state. Time-resolved fluorescence data support assignment of this band to the emissive singlet state, whose dynamic characteristics depend strongly on the dielectric strength of the medium. On the basis of all our time-resolved measurements combined with simulations of the observed kinetics, we propose the following model: the initially populated S_2 state decays to the S_1 state within less than 100 fs for both solvents. Then, the population is transferred from the S_1 state to the S_0 and ICT states. The $S_1 \rightarrow$ ICT transfer is controlled by a solvent polarity dependent barrier. In *n*-hexane the barrier is high enough to prevent the $S_1 \rightarrow$ ICT transfer and only $S_1 \rightarrow S_0$ relaxation characterized by a time constant of 160 ps is observed. An increase of solvent polarity leads to a significant decrease of the barrier, enabling a direct quenching of the S_1 state by means of the $S_1 \rightarrow$ ICT transfer, which is characterized by a time constant of 148 ps for tetrahydrofuran, 81 ps for 2-propanol, and 11 ps for the most polar solvent methanol. The ICT state is then rapidly depopulated to the ground state. This relaxation also exhibits solvent dependence, having a time constant of 1 ps in methanol, 2.5 ps in 2-propanol, and 3.5 ps in tetrahydrofuran.

1. Introduction

Carotenoids play a number of roles in living organisms. In addition to their well-known function as light-harvesting pigments in photosynthesis,[1] they are important components of the photoprotection mechanism in plants[2] and are antioxidants that prevent damage to various physiological systems by quenching triplet states and radicals.[3] The key energetic feature of carotenoids is an atypical order of energy levels, making the transition to the lowest energy state optically forbidden. Because the conjugated chain of the carotenoid molecule has C_{2h} point symmetry, a transition between the $1A_g^-$ state (ground state, S_0) and the $1B_u^+$ (S_2) state is allowed, while the $1A_g^- \rightarrow 2A_g^-$ ($S_0 \rightarrow S_1$) transition is forbidden for one-photon processes.[4,5] However, as shown for the first time three decades ago for short polyenes,[6,7] due to strong electron correlation the $2A_g^-$ state has actually a lower energy than the $1B_u^+$ state; thus it is the transition to the lowest energy state that is forbidden. Indeed, the $1A_g^- \rightarrow 1B_u^+$ transition accounts for the strong absorption in the spectral region 400−550 nm characteristic of carotenoids.[1] Studies of dynamics of carotenoid excited states have established the following scheme: after excitation of a carotenoid to its S_2 state ($1B_u^+$), a fast relaxation to the S_1 state ($2A_g^-$) occurs on a time scale of 50−300 fs.[8−10] Subsequently, the carotenoid relaxes to its ground state S_0 due to vibronic coupling between the S_0 and S_1 states[11] on the time scale of 1−300 ps.[12] There is a clear correlation between the S_1 lifetime and the conjugation length of carotenoids: as the conjugation length increases, the energy gap between the S_0 and S_1 state becomes smaller, thereby making the S_1 lifetime shorter. Because of the negligibly small dipole moment of the S_1 state, it was generally believed that the lifetime of the S_1 state demonstrates very little solvent dependence.

Peridinin is a highly substituted carotenoid occurring in some dinoflagellates, where it is the principle carotenoid of both the membrane bound light harvesting protein and the water-soluble light-harvesting peridinin−chlorophyll−protein (PCP). The structure of the PCP complex from *Amphidinium carterae*, which has been resolved to 2.0 Å by X-ray crystallography,[13] exhibits an exceptional stoichiometry: 8 peridinins and 2 chlorophyll *a* (Chl-*a*). Peridinin, as shown in Figure 1 has a C37 carbon skeleton (rather than the usual C40 system found in most carotenoids) together with an allene moiety, lactone ring and carbonyl group. This unusual carotenoid structure together with the high-resolution structure of PCP has become the focus of a number of spectroscopic studies.[14−18]

† This work was presented at the PP2000 in Costa do Estoril, Portugal, honoring Professor Ralph Becker's contributions.

* Corresponding author. E-mail: villy.sundstrom@chemphys.lu.se. Fax: +46−46−2224119.

‡ Lund University.

§ Macquarie University.

10.1021/jp010022n CCC: $20.00
Published on Web 06/05/2001

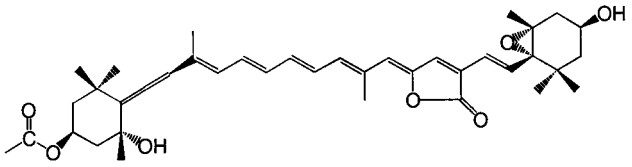

Figure 1. Molecular structure of peridinin.

Early work on peridinin demonstrated that its structure leads to breaking of the idealized C_{2h} symmetry, resulting in relatively strong fluorescence from the S_1 state[19] and established a rather long S_1 lifetime of 103 ps when measured in carbon disulfide.[20] However, three recent studies of peridinin dissolved in various solvents of different polarity by Frank and co-workers[14−16] showed a clear dependence of the peridinin S_1 lifetime on the solvent polarity. They also reported peridinin transient absorption spectra taken at a 5 ps delay time in the region from 500 to 750 nm in solvents with different polarity.[15] The transient absorption spectrum of peridinin in *n*-hexane possesses two spectral bands: one located at ∼510 nm and another at ∼660 nm, while in methanol only one broad band at ∼590 nm is present. They attributed the absorption bands at 510 and 660 nm in *n*-hexane to the $S_1 \rightarrow S_n$ transition and to the transition from an additional low-lying state to some $S_{n'}$ state, respectively. The band observed at 590 nm in methanol was ascribed solely to the transition from the new state to the $S_{n'}$ state. By comparing with time-resolved studies on other molecules, a model was proposed in which the presence of a new state with charge-transfer (CT) character in the excited state manifold plays a crucial role in polar solvents. The CT state was suggested to lie below the S_1 state of peridinin, resulting in quenching of the S_1 state and hence to a shorter S_1 lifetime in polar solvents. Initially, the CT state was ascribed to the presence of the lactone ring,[15] but a subsequent study of other carotenoids showed a similar (but less pronounced) behavior for fucoxanthin, which has an allene moiety and a carbonyl group but lacks a lactone ring, and for uriolide acetate, which has a lactone ring but lacks an allene moiety.[16]

In addition to the S_1 lifetime dependency, there is a striking difference between absorption spectra in polar and nonpolar solvents. For carotenoids with a strong S_1 lifetime dependence on solvent polarity, the characteristic three-peak vibrational structure of the $S_0 \rightarrow S_2$ transition is lost in polar solvents and a rather broad and structureless absorption band is observed.[16] Interestingly, loss of vibrational structure in polar solvents is also observed for the carotenoid spheroidenone, although the S_1 lifetime is not changed. A similar behavior of the $S_0 \rightarrow S_2$ transition was found for a series of apocarotenoids substituted with various terminal groups also containing a carbonyl group.[21]

Analogous to carotenoid → (bacterio)chlorophyll energy transfer in many light-harvesting complexes,[22−25] the efficiency of peridinin → Chl-*a* transfer in the PCP complex is quite high.[14,18,20] In LH2 from purple bacteria[22,23] or LHC from higher plants,[24,25] the energy pathway via the carotenoid S_2 state usually plays a dominant role, whereas peridinin → Chl-*a* energy transfer in PCP occurs predominantly via the S_1 state. To fully understand the mechanism of such efficient energy transfer via the S_1 state, knowledge of the excited state dynamics associated with the S_1 state together with the behavior and origin of the CT state of peridinin in solution is necessary.

Here we report the application of various time-resolved spectroscopic techniques for the study of the energetics and dynamics of the lowest excited states of peridinin in polar and nonpolar solvents. The results are based mostly on a recently introduced experimental approach enabling us to locate the S_1 excited state of carotenoids and monitor its dynamics by scanning the $S_1 \rightarrow S_2$ excited state absorption in the near-infrared region.[26] Together with time-resolved fluorescence measurements these results enabled us to assemble a more complete picture of the peridinin excited state dynamics, which will be discussed in detail.

2. Experimental Section

Sample Preparation. Pigments were extracted from washed thylakoid membranes of *A. carterae* by the procedure of Martinson and Plumley[27] except that 1-butanol was used in place of 2-butanol. Peridinin was separated by HPLC on a C18 Econosil column 250 × 10 mm (Alltech) using a two-solvent gradient. Solvent A was 50% water/25% methanol/25% acetonitrile and solvent B was 50% methanol/50% acetonitrile. The column was equilibrated with 80% B. The sample was applied at a flow rate of 1.5 mL/min, this flow rate was held for 5 min, and then B was gradually increased to 99% over 20 min; the flow rate was then increased to 3 mL/min until Chl-*a* eluted. The eluent was monitored at 440 nm, and the fractions containing peridinin were dried under vacuum in darkness and stored at −20 °C. Chl-*c* emerged close to the void volume and characteristic retention times were peridinin 17.4 min, diadinoxanthin 23.8 min, and Chl-*a* 39.8 min.

Before the experiments, peridinin samples were dissolved in different solvents to yield an optical density of ∼0.1 OD at the excitation wavelength for the streak-camera measurements, ∼0.5 OD for the fluorescence upconversion, and ∼0.3 OD for the transient absorption measurements. All measurements were performed in a 2 mm optical path length glass cuvette at 293 K. Solvents used were *n*-hexane, methanol, tetrahydrofuran, diethyl ether, and 2-propanol, all obtained from Merck, and carbon disulfide was from AnalaR.

Time-Resolved Optical Spectroscopy. *Streak-Camera Measurements.* Excitation pulses were obtained by frequency doubling of the Ti:sapphire femtosecond oscillator output with a 1.5 mm KDP nonlinear crystal. The Ti:sapphire oscillator operated at 81 MHz repetition rate and was pumped by the 8 W output of a continuous-wave (CW) frequency-doubled, diode-pumped Nd:YVO_4 laser. The excitation pulses had a duration of ∼150 fs and energy of 3.7−7.5 pJ/pulse in the wavelength range 450−480 nm. The ultimate time resolution of the streak-camera was 1.3 ps after dispersion of the spectrum by a 0.25 m spectrograph. Time and wavelength dependence of the fluorescence intensity was measured simultaneously in a 3D window, where the vertical axis corresponded to time, the horizontal axis corresponded to wavelength, and the fluorescence intensity was color coded. Transient fluorescence spectra were measured in time ranges from 100 to 1000 ps depending on the fluorescence decay time of the samples, and the fwhm of the response function of the streak camera varied from 2 to 10 ps, correspondingly. All measured fluorescence spectra were corrected for shading and spectral sensitivity of the apparatus. Test experiments showed that both fluorescence kinetics and spectra were independent of the mutual polarization of excitation and fluorescence light, so all streak-camera measurements reported here were performed without polarization settings.

Fluorescence Upconversion Technique. Subpicosecond fluorescence upconversion measurements were performed in a standard experimental setup, which is briefly described below. The same Ti:sapphire-based laser system as employed for the streak-camera measurements was used. After the frequency doubling in the 1.5 mm KDP crystal, pulses were split by a dielectric beam splitter to produce an ∼7.5 nJ gate pulse centered

at 940 nm and an ~160 pJ excitation pulse at 470 nm. A long-wavelength cutoff filter was inserted in the excitation beam to block residual 940 nm light. After the sample, a short-wavelength cutoff filter was used to prevent excitation light from entering the detection system. The time delay between the excitation and gate pulses was changed by a computer-controlled optical delay line. Fluorescence was collected by a microscope objective and mixed with the gating light in a 0.5 mm BBO type I crystal by a 50 mm focal length quartz lens. The generated sum-frequency signal was separated from fluorescence light, transmitted excitation and frequency-doubled gate light by an aperture. Remaining undesired light was minimized by a 10 nm band-pass interference filter and a single grating monochromator. The generated sum-frequency was detected by employing a single photon counting technique by a cooled (−5 °C) photomultiplier tube and photon counter. Multiple scans of the decay were summed until a desired signal-to-noise ratio was reached. In all measurements, the mutual polarization of the excitation and gate beams was set to the magic angle (54.7°) using a polarization rotator placed in the gate beam. A typical pump-gate cross correlation function measured by mixing gate and pump beams in a 0.5 mm BBO crystal had a fwhm of 240−250 fs, and a fitted Gaussian shaped instrument response function was used in fitting the kinetics. The small effect of the different group velocity mismatch between the fluorescence and the gate pulse[28] at different fluorescence wavelengths was neglected.

Pump−Probe Apparatus. Two similar femtosecond spectrometers were used in visible and near-infrared pump−probe measurements. Both systems were based on an amplified Ti:sapphire laser system.

For the visible range measurements, femtosecond pulses were obtained from a Ti:sapphire oscillator pumped by the 5 W output of a CW frequency-doubled, diode-pumped Nd:YVO_4 laser. The oscillator, operating at a repetition rate of 82 MHz, was amplified by a regenerative Ti:sapphire amplifier pumped by a Nd:YLF laser (1 kHz), producing 120−160 fs pulses with an average energy of ~1 mJ/pulse and a central wavelength at 800 nm. For measurements of transient absorption spectra in the spectral range 470−740 nm, the amplified pulses were divided into two paths: one to pump an optical parametric amplifier for generation of pump pulses at 490 nm, and the other to produce white-light continuum probe pulses in a 0.5 cm sapphire plate. The mutual polarization of the pump and probe beams was set to the magic angle (54.7°) using a polarization rotator placed in the pump beam. For signal detection, the probe beam and an identical reference beam (that had no overlap with the pump beam) were focused onto the entrance slit of a spectrograph, which then dispersed both beams onto a home-built dual photodiode array (PDA) detection system. Each array contained 512 photodiodes and allowed a spectral range of ~270 nm to be measured in each laser shot. Every millisecond readout of all photodiodes was converted by a 16-bit analog to digital converter (ADC) and transferred to the computer. The spectral resolution of the detection system was ~100 cm^{-1} and the energy of excitation was ~150 nJ/pulse, giving an excitation density of ~10^{15} photons $pulse^{-1}$ cm^{-2}. Chirp compensation of the spectra was performed manually after the measurements.

For the infrared pump−probe measurements femtosecond pulses were obtained from a Ti:sapphire oscillator pumped by the 9 W output of a CW Ar^+ laser. The oscillator (82 MHz) was amplified by a regenerative Ti:sapphire amplifier pumped by a Nd:YLF laser (5 kHz), producing 120−160 fs pulses with an average energy of ~200 μJ/pulse and a central wavelength at 800 nm. The amplifier output was divided by a 75/25 beam splitter to pump two independent optical parametric amplifiers for generation of the pump and probe pulses. The wavelength of the pump pulses was fixed at 490 nm, while the wavelength of the probe pulses was scanned over the spectral region 700−1900 nm by a computer-controlled parametric amplifier. The mutual polarization of pump and probe beams was set to the magic angle. The detection system was based on a three-photodiode arrangement (probe, reference and pump) in combination with a single grating monochromator and gave a spectral resolution of 40 cm^{-1}. The energy of the pump pulses was kept below 40 nJ/pulse, corresponding to an excitation density of ~10^{14} photons $pulse^{-1}$ cm^{-2}.

For all measurements in the visible as well as in the near-IR range the instrument response function was measured by frequency mixing the pump and probe pulses in a 1.5 mm KDP crystal and the obtained cross-correlation was fitted by a Gaussian function with a fwhm of 160−180 fs, depending slightly on the wavelength of the probing pulses. This Gaussian function was used as the instrument response function for the multiexponential fitting procedure.

Absorption spectra were measured before and after all kinetic measurements to monitor whether photochemical changes occurred during the experiment. No sample degradation was observed during the course of kinetic measurements, except for the fluorescence upconversion measurements of peridinin in *n*-hexane. Here, due to extremely weak signals the accumulation time was as long as 8 h and, after the measurement, the sample absorption maximum was reduced by 30−50%. This was due to deposition of some carotenoid molecules on the cuvette walls as well as degradation of the sample.

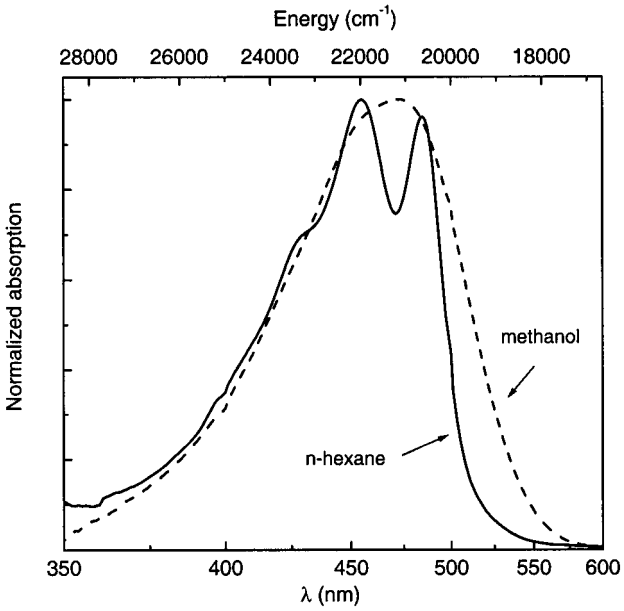

Figure 2. Peridinin absorption spectra in *n*-hexane (solid line) and methanol (dashed line). Both spectra are normalized to their absorption maxima.

3. Results

Steady State Absorption. Absorption spectra of peridinin in two solvents of different polarity, *n*-hexane (nonpolar) and methanol (polar), are shown in Figure 2. Absorption in the 350−550 nm region is associated with the strongly allowed $S_0 \rightarrow S_2$ transition and in *n*-hexane exhibits a well-resolved vibronic structure. The separation between vibrational peaks of ~1350

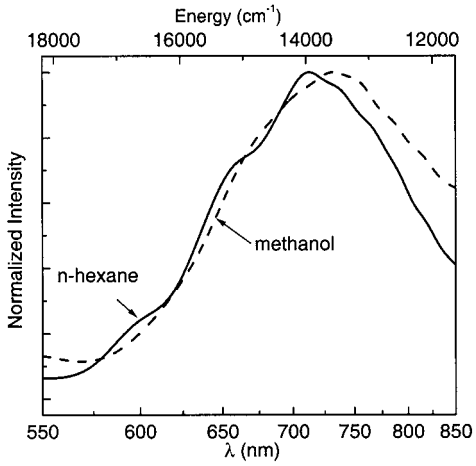

Figure 3. Integrated peridinin fluorescence spectra: (solid line) in *n*-hexane (excitation at 455 nm, integrated over 300 ps); (dashed line) methanol (excitation at 473 nm, integrated over 30 ps).

cm^{-1} results from the combination of two symmetric vibrational modes with energies of 1150 cm^{-1} (C−C stretch) and 1600 cm^{-1} (C═C stretch). In contrast, the vibronic structure is completely lost in methanol and the absorption band is significantly wider. From the spectrum of peridinin in *n*-hexane, the positions of vibrational bands can be evaluated and are as follows: 0−0 transition, 485 nm (20620 cm^{-1}); 0−1 transition, 455 nm (21980 cm^{-1}); 0−2 transition, 429 nm (23310 cm^{-1}).

Time-Resolved Fluorescence. Time-resolved fluorescence streak-camera measurements of peridinin in several solvents with different polarities were performed. Because the symmetry of the peridinin molecule deviates significantly from the idealized C_{2h} point group, the optical $S_1 \rightarrow S_0$ transition is not totally forbidden and dual fluorescence can be observed from the S_2 and S_1 states. However, the S_2 state fluorescence decay is very fast, less than 100 femtoseconds, and cannot be resolved with the time resolution of the streak-camera (∼1 ps). The integrated S_1 fluorescence spectra measured in methanol and *n*-hexane are shown in Figure 3. Both spectra were smoothed by a low-frequency FFT filter. The integration time was selected to achieve the best signal-to-noise ratio and was always longer than the lifetime of the fluorescence decay. The excitation wavelength was tuned to the maximum of the steady state absorption spectrum. The fluorescence spectrum measured in *n*-hexane exhibits some vibronic structure, while in methanol the spectrum is rather broad and structureless. Since it is known that for carotenoids the maximum of the fluorescence spectrum is usually due to the 0−2 vibronic band,[5] a decomposition of the fluorescence spectrum of peridinin in *n*-hexane into Gaussian bands gives an S_1 state energy of peridinin in *n*-hexane of about 16 700 cm^{-1}. Since there is no vibronic structure observed for peridinin in methanol, we can only estimate the position of the S_1 level on the basis of knowledge of the energy gap between vibrational modes (∼1350 cm^{-1}). The fluorescence spectrum of peridinin in methanol peaks at 715 nm and corresponds to S_1 energy of ∼16 300 cm^{-1} in methanol assuming the maximum is due to the 0−2 vibrational band. An interesting feature of the fluorescence spectra shown in Figure 3 is the increase of fluorescence intensity with solvent polarity at the low-energy edge of the fluorescence spectrum. This behavior is in agreement with transient absorption measurement (see below) and will be analyzed in detail in the Discussion. In addition to the time-integrated spectra shown in Figure 3, which actually correspond to steady state fluorescence spectra, we have measured complete dynamics of the fluorescence spectra in both solvents and have not observed any spectral evolution on the time scale given by the resolution of streak-camera.

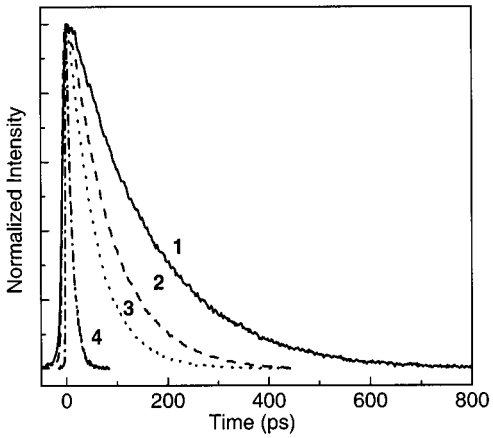

Figure 4. Kinetic traces of peridinin fluorescence in different solvents taken at 730 nm: (1) in *n*-hexane (τ = 156 ps); (2) in tetrahydrofuran (τ = 77 ps); (3) in 2-propanol (τ = 54 ps); (4) in methanol (τ = 10.5 ps). All traces are normalized.

TABLE 1: Solvent Polarity Factors, $P(\epsilon) = (\epsilon - 1)/(\epsilon + 2)$, Peridinin Lifetimes Measured by Time-Resolved Fluorescence Measurements (τ), and Lifetimes Measured by Transient Absorption[15] (τ*)

solvent	$P(\epsilon)$	τ (ps)	τ* (ps)
n-hexane	0.299	156 ± 3	161
carbon disulfide	0.354	173 ± 3	168
diethyl ether	0.526	150 ± 3	157
tetrahydrofuran	0.687	77 ± 3	79
2-propanol	0.852	54 ± 2	51
methanol	0.913	10.5 ± 1	12

The S_1 state fluorescence kinetics of peridinin taken at 730 nm in solvents of different polarity are shown in Figure 4, where the dramatic dependence of the S_1 state fluorescence lifetime on solvent polarity is evident. The lifetime changes more than 1 order of magnitude, from 156 ps in *n*-hexane to 10.5 ps in methanol. In all solvents, kinetic traces could be fitted by a single exponential decay independent of detection wavelength over nearly the entire fluorescence band (650−850 nm). In the spectral region from 550 to 650 nm, the fluorescence decay was fitted by two exponentials, one of which was the same as for the longer wavelengths and corresponded to the S_1 relaxation, and another corresponding to the very fast decay of the S_2 state. The $S_2 \rightarrow S_1$ relaxation time for peridinin in ethanol was measured by the upconversion technique,[29] giving an S_2 lifetime of 43 fs. In addition, our recent pump−probe experiments with 30 fs time resolution give an S_2 lifetime of ∼60 fs for peridinin in methanol and ∼30 fs for peridinin in *n*-hexane.[30] Thus, the decay of the S_2 state is clearly beyond the time resolution of the streak-camera.

The peridinin excited state lifetimes together with polarity factors of the solvents used, are summarized in Table 1. The polarity factors were calculated from the dielectric constant of the solvents, using the expression $P(\epsilon) = (\epsilon - 1)/(\epsilon + 2)$. The lifetimes obtained from our streak-camera measurements coincide very well with recent results obtained from transient absorption measurements by Bautista et al.,[15] indicating that the same state is observed in both types of measurements and that this state exhibiting strong solvent dependence is the emissive state of peridinin. This conclusion is further supported by our transient absorption measurements presented below.

Transient Absorption. Transient absorption spectra of peridinin in *n*-hexane and methanol were measured in two different

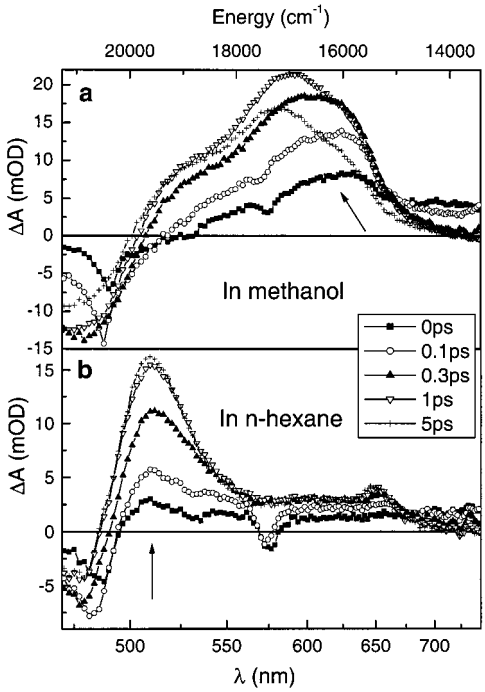

Figure 5. Transient absorption spectra of peridinin in methanol (a) and *n*-hexane (b) at different time delays after the excitation at 490 nm. Corresponding delay times are shown in an inset. The arrows indicate evolution of the signal.

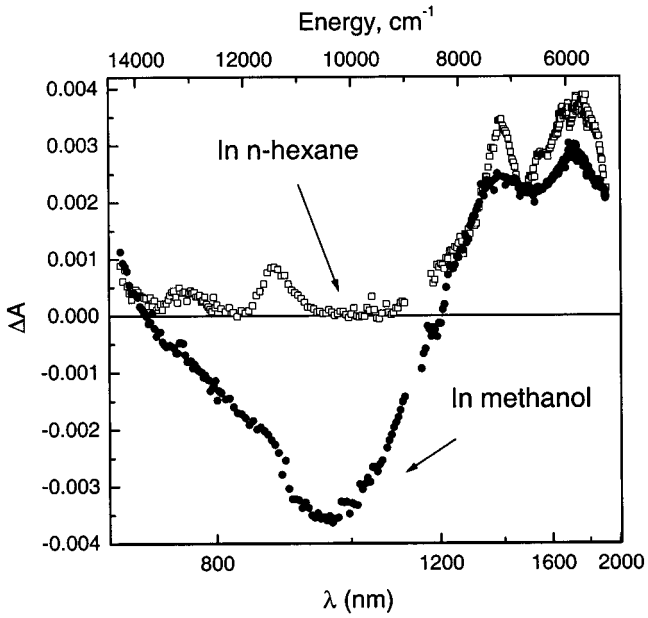

Figure 6. Peridinin near-IR transient absorption spectra in *n*-hexane and methanol. Delay time is 1 ps after the excitation. Samples were excited at 490 nm.

spectral regions: the visible region from 470 to 740 nm and the near-infrared region from 700 to 1900 nm. In both cases, peridinin was excited into the low-energy wing of the 0−0 vibronic band of the $S_0 \rightarrow S_2$ transition at 490 nm, to avoid any contributions from relaxation within the S_2 state vibrational manifold.

Transient absorption spectra in the visible spectral region are shown in Figure 5 for the first 5 ps after excitation. In hexane, two excited state absorption (ESA) bands are observed in the transient absorption spectrum: a strong sharp band centered at ∼510 nm and a weaker one located at ∼650 nm. Both these bands exhibit the same dynamics and have been observed previously.[15] For peridinin in methanol, however, the observed dynamics is much more complex. A rather structureless spectrum observed at zero delay evolves within 100 fs into a transient spectrum exhibiting a main maximum around 630 nm with a shoulder at 530 nm. The spectral positions of these two bands resemble the ESA bands observed for peridinin in *n*-hexane. Both these bands are significantly broader than those observed in *n*-hexane, most likely as a reason of the S_n state broadening. The opposite ratio of the amplitudes of the bands when compared to *n*-hexane can be explained by a significant bleaching signal above 500 nm for peridinin in methanol, canceling the ESA signal in the region 500−550 nm. In addition to that, stimulated emission from the S_2 state can affect the actual shape of the observed bands at early delay times. Superimposed on these two $S_1 \rightarrow S_n$ bands, a new band appears at longer delay times. This band is centered at ∼590 nm at 1 ps and is shifted to a final position at ∼575 nm in 5 ps. For both methanol and *n*-hexane solutions, the ESA signal in the red-most part of the transient absorption spectrum (>675 nm) exhibits an instantaneous rise followed by subpicosecond decay. This ESA has been already observed for other carotenoids and is most likely due to a transition from the initially populated S_2 state to some higher excited state.[31]

The negative features in the transient absorption spectra observed in both solvents are due to either ground state bleaching (BL) or stimulated emission (SE) from the excited state. The negative band centered around 480 nm is the bleaching of the ground state. Since this band reflects the shape of the $S_0 \rightarrow S_2$ transition, it is significantly sharper in *n*-hexane, where the vibronic structure is preserved. In both cases, the bleaching band exhibits an instantaneous rise and then decays with the same lifetime as the ESA. There are also sharp negative features observed in both methanol and *n*-hexane at 574 and 531 nm. Both these bands demonstrate an instantaneous rise and disappear within 300 fs. The energy separation between the excitation wavelength (490 nm) and these bands is ∼1580 and ∼3000 cm^{-1}. Transient absorption experiments of pure methanol and *n*-hexane under the same conditions were carried out (data not shown) to clarify the origin of those bands. Data obtained in both solvents are very similar and reveal a strong sharp negative band centered at 571 nm and another one approximately 5 times weaker at 520 nm. Both bands are attributed to stimulated Raman scattering and feature the same dynamics as observed in the experiments with peridinin at 574 and 531 nm. Thus, we suggest that the bands observed for peridinin solution originate from stimulated Raman scattering by the solvent and a resonance Raman signal from the carotenoid. Both bands could be a combination of different Raman signals, but apparently the 574 nm band is mostly caused by the Raman scattering from the solvent and the 531 nm band comes from Raman signal of peridinin (a shift from the excitation wavelength of 1580 cm^{-1} is very close to the Raman active double bond vibration frequency of 1600 cm^{-1}).

Near-IR transient absorption spectra of peridinin in *n*-hexane and methanol were measured in the spectral range extending from 700 to 1900 nm (see Figure 6). At 1 ps most of the peridinin molecules are in the S_1 state, since the $S_2 \rightarrow S_1$ relaxation occurs on a time scale faster than 100 fs[29,30] and the S_1 lifetime is more than 1 order of magnitude longer in both solvents. In the red-most part of the transient spectrum, the signal is dominated by the $S_1 \rightarrow S_2$ transition, with the two vibronic peaks having the same separation (1320 ± 50 cm^{-1}) as for the vibronic bands of the strongly allowed $S_0 \rightarrow S_2$ transition (Figure 2). It should be noted that the vibronic structure of the $S_1 \rightarrow S_2$ transition is better resolved in *n*-hexane than in methanol, in

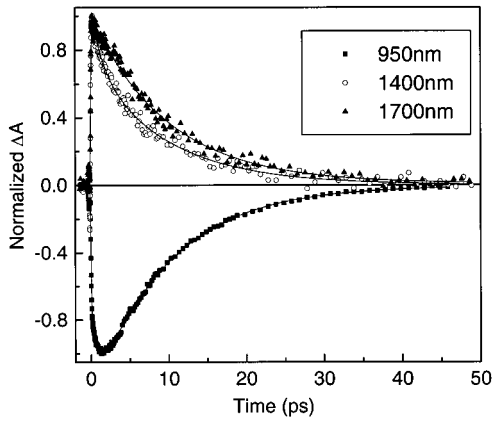

Figure 7. Peridinin transient absorption kinetics in methanol. Squares, circles, and triangles are the traces measured at 950, 1400, and 1700 nm, correspondingly. Lines represent multiexponential fits. Excitation was at 490 nm. Traces are normalized either to the positive or to the negative maximum of the signal.

good accordance with steady state absorption and fluorescence spectra. Otherwise, the shape of the $S_1 \rightarrow S_2$ profile is quite similar in both solvents.

The most interesting part of the near-IR peridinin transient absorption spectrum is the spectral region between 720 and 1200 nm and its solvent dependence. In *n*-hexane, this region exhibits two weak ESA bands centered at 875 and 760 nm. Kinetic traces measured at these bands show the same dynamic behavior as the traces measured at energies corresponding to the $S_1 \rightarrow S_n$ transition. This implies that the bands can be assigned to a transition from the S_1 state to some higher states lying between the S_2 and S_n states. It is important to note that these bands must actually be superimposed on a rather broad ESA band, because a significant ESA is required to cancel the S_1 emission in this spectral region (see Figure 3). More complex spectral characteristics are revealed in the same region when peridinin is dissolved in methanol: a broad structureless SE band centered at ~980 nm dominates the transient absorption spectrum. A closer inspection of this SE band shows that the weak ESA features clearly seen in *n*-hexane are also present in methanol, superimposed on the broad and strong negative feature. As discussed in detail below, this SE band observed in methanol is due to stimulated emission from an additional state with CT character, which is stabilized in a polar environment.

Kinetic traces of peridinin in the spectral region 600−1900 nm measured in both solvents reveal characteristic decay times of 10 ± 1.5 ps (methanol) and 160 ± 15 ps (*n*-hexane), which are in very good agreement with the streak-camera measurements. They are clearly the lifetimes of the S_1 state, since they are the same at all wavelengths. In *n*-hexane, kinetics measured over the whole spectral range display a single-exponential decay, except the wavelength interval 700−1200 nm, where an additional ultrafast (<200 fs) decay component is detected due to ESA from the $S_2 \rightarrow S_n$ transition.[30] In methanol the observed dynamics are more complex (Figure 7). Kinetics measured within the strong SE band exhibit an additional rise component with a time constant of ~1 ps. At the maximum of the SE band this component has an amplitude of 39% of the whole rise. The same rise component is observed also at the maximum of the $S_1 \rightarrow S_n$ transition (600 nm) with about the same amplitude as at the SE maximum. At the high-energy edge of the $S_1 \rightarrow S_2$ transition (between 1160 and 1315 nm) this time constant is observed as a decay component as the result of the interplay between the SE and ESA signals. Since there is an overlap of ESA and SE bands, the rise of stimulated emission is actually observed as a decay component of the positive ESA-dominated signal. The observation that there is no 1 ps component present at the very low energy edge of the IR transient spectrum (>1515 nm) constitutes strong support for this conclusion. Likewise, in *n*-hexane, some of the traces required an ultrafast component of ≤0.1 ps to account for the $S_2 \rightarrow S_1$ internal conversion. All fitting parameters of the kinetics measured in methanol at different wavelengths extending from 600 to 1800 nm are summarized in Table 2. In addition, there are fitting parameters of peridinin kinetics in *n*-hexane at both infrared band maxima included in Table 2.

TABLE 2: Time Constants (τ_1, τ_2, τ_3) and Corresponding Relative Amplitudes (A_1, A_2, A_3) Extracted from Multiexponential Fits of the Kinetics of Peridinin in Methanol and *n*-Hexane[a]

λ (nm)	E (cm^{-1})	τ_1 (ps)	A_1 (%)	τ_2 (ps)	A_2 (%)	τ_3 (ps)	A_3 (%)
			In Methanol				
600	16 670			1	−34.6	9.7	100
700	14 290	<0.1	92.2	1.5	−1.4	8.8	7.8
950	10 530			1	−38.4	9.6	100
1050	9520	<0.1	85.9	0.9	−14.1	10.1	21.5
1150	8700	<0.1	81.0	1.1	−19.0	9.8	16.3
1300	7690	<0.1	90.3	1.4	5.3	10.1	4.4
1400	7140			1.4	27.0	9.1	73.0
1500	6670			1.3	17.1	12.0	82.9
1600	6250	<0.1	−90.6			9.6	100
1700	5880					9.8	100
1800	5560	<0.1	−88.1			10.2	100
			In *n*-Hexane				
1400	7140					152	100
1800	5560					168	100

[a] Negative amplitudes correspond to the rise and positive to the decay. The component (τ_1, A_1) is due to very fast relaxation of the S_2 state; the time constant of this component could not be resolved by the experimental setup. Uncertainties of the lifetimes and amplitudes vary from ±5% to ±10%.

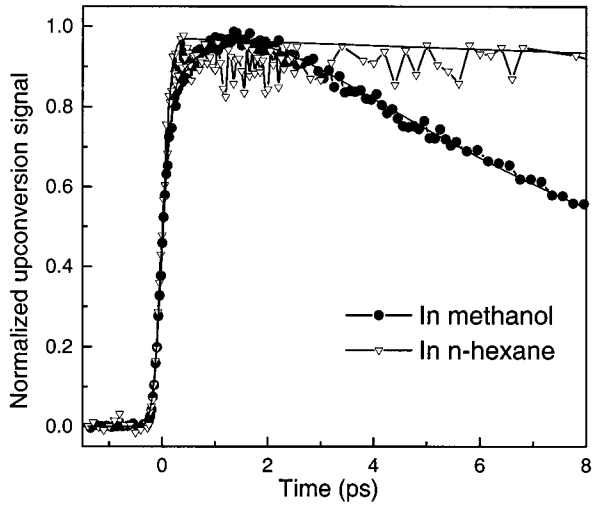

Figure 8. Rise of the peridinin fluorescence kinetics in methanol and *n*-hexane measured by fluorescence upconversion at 793 nm. Solid lines correspond to the fits. Excitation was at 470 nm. Traces are normalized to the maximum.

Fluorescence Upconversion Kinetics. To further clarify whether the 1 ps kinetic component obtained from the transient absorption measurements in methanol indeed originates from an emissive state, we performed fluorescence upconversion measurements of peridinin in methanol and *n*-hexane. As shown in Figure 8, in *n*-hexane, upconversion kinetics in the spectral range 760−827 nm exhibit an instantaneous rise (with a time resolution of ~200 fs) followed by the slow decay of (~200

TABLE 3: Fitting Parameters of the Fluorescence Upconversion Kinetics for Peridinin Excited at 470 nm[a]

λ (nm)	τ_2 (ps)	A_2 (%)	τ_3 (ps)	A_3 (%)
727	1	−16	10.1	100
760	1	−28	9.9	100
793	1.1	−36	9.5	100
827	1	−40	9.6	100

[a] In addition to the finite rise component (τ_2, A_2), part of the rise is instantaneous. Uncertainties for the lifetimes and amplitudes are within ±5%.

ps) of the S_1 state fluorescence. This S_1 lifetime obtained from the fitting procedure is somewhat longer than that measured by streak-camera and pump−probe techniques, and is probably due to very small signals and a rather poor signal-to-noise ratio in the upconversion experiments. For peridinin in methanol, kinetic traces in the wavelength range 727−827 nm show a clear rise component with a time constant of 1 ps, in good agreement with the rise time obtained from the transient absorption kinetics. The rest of the fluorescence rise is instantaneous and the amplitude of the 1 ps component increases gradually with probing wavelength, reaching as much as 40% at 827 nm. The decay of upconversion signal in all spectra region 727−827 nm is well fitted by an ∼9.8 ± 0.3 ps component corresponding to the S_1 lifetime. All time constants and amplitudes extracted from the upconversion measurements of peridinin in methanol are summarized in Table 3.

4. Discussion

The measurements of transient absorption spectra in the visible spectral region (500−700 nm) show that dynamic spectral changes of the transient absorption band in this region observed in methanol contrast strongly with the time independent shape of the transient spectrum measured in *n*-hexane. It is clear from Figure 5 that the new ESA band appearing in the transient absorption maximum in methanol within 1 ps is shifted by ∼1100 cm^{-1} and after 5 ps by ∼1300 cm^{-1} from the ESA band, which appears instantaneously. The transient absorption spectrum, especially at delay times longer than 0.7 ps, has an apparent three-peak substructure, which could be interpreted as vibronic bands. The shift in the transient absorption spectrum, as seen in Figure 5, might then be interpreted as vibrational cooling of the S_1 state or redistribution of the population of peridinin molecules from the higher to lower vibrational levels, as the observed spectral evolution corresponds to a blue shift of the transient absorption maximum. However, since no similar dynamics were detected in *n*-hexane, the above explanation is rather unlikely. Following a similar argument as in Bautista et al.,[15] the strong difference between the transient spectra in methanol and in *n*-hexane can be explained in terms of the transfer of the population from the S_1 state to a new state, most likely with charge-transfer character, which is stabilized in the polar solvent methanol. As this state would lie below the S_1 state of peridinin, it efficiently quenches the S_1 state, leading to both a significant shortening of the S_1 lifetime in polar solvents and a decrease of the fluorescence quantum yield. Though the transient absorption signal in the visible region is complex, the two ESA bands located at 630 and 530 nm are most likely due to the excited state absorption from the S_1 state, while the new band centered at 575 nm is a result of a transition from the CT state, which is not observed in *n*-hexane. It should be noted that we have no definitive information about the final S_n state, which can consist of a group of higher states. We also have no information about possible solvent-induced shifts of this state (states). Therefore, we cannot determine if the final S_n state is the same for both $S_1 \rightarrow S_n$ and CT $\rightarrow S_n$ transitions. Thus, the value of 1300 cm^{-1} mentioned above can be taken only as a rough estimate of the energy difference between S_1 and CT states.

Light-induced absorbance changes in the 500−700 nm spectral region primarily provide information about the transition from the S_1 and the state with CT character to the S_n state. As discussed above, this region is useful for monitoring dynamics of the S_1 state, but to determine the energy of the S_1 state of peridinin a better defined transition is required. The near-IR spectral region, probing the $S_1 \rightarrow S_2$ transition is an ideal tool for this purpose[26] and by applying a near-IR transient absorption technique, the energies of the S_1 state of several carotenoids were evaluated.[26,31] Figure 6 shows the results of the near-IR measurements of peridinin in *n*-hexane and methanol. For the determination of the S_1 level energy, assignment of the observed bands to the vibronic bands of the $S_1 \rightarrow S_2$ transition is crucial.[26,31] In the near-IR region of the transient absorption spectra of peridinin in *n*-hexane and methanol shown in Figure 6, two vibronic bands located at 5870 ± 100 and 7190 ± 100 cm^{-1} are present. Since we know from fluorescence spectra that the energy of the S_1 level is about 16 700 cm^{-1}, a simple calculation of the S_1-S_2 energy gap leads to the energy of the 0−0 vibronic band of the $S_1 \rightarrow S_2$ transition of about 4500 cm^{-1}, which is beyond the sensitivity range of our experimental setup. Therefore, we attribute the peaks observed in the near-IR absorption spectrum to the 0−1 and 0−2 vibronic bands of the $S_1 \rightarrow S_2$ transition. Then, we can calculate the S_1 energy also from the $S_1 \rightarrow S_2$ transition by a simple subtraction $E(S_0 \rightarrow S_2) - E(S_1 \rightarrow S_2)$. Using the energies of the $S_0 \rightarrow S_2$ and $S_1 \rightarrow S_2$ 0−1 absorption transitions, we calculate the energy of the S_1 state of peridinin in *n*-hexane to be 16 100 ± 200 cm^{-1}. It is important to note that such a calculation of the S_1 energy gap is reasonable only for peridinin in *n*-hexane, because the steady state absorption spectrum of peridinin in methanol is structureless and it is therefore difficult to read the energy of the 0−0 origin from the $S_0 \rightarrow S_2$ transition. If one nevertheless attempts to estimate the S_1 energy of peridinin in methanol, the absorption spectrum in *n*-hexane can be used to estimate the S_2 energy in methanol. With this approximation, we obtain the S_1 energy of peridinin in methanol to be 16 100 ± 500 cm^{-1}. Changing the assignment of the bands observed in the $S_1 \rightarrow S_2$ spectrum to be the 0−2 and 0−3 transitions would lead to an S_1 energy of 17 450 ± 200 cm^{-1} in *n*-hexane. Taking into account the experimental errors, none of the assignments gives the S_1 energy of 16 700 ± 200 cm^{-1} obtained from the fluorescence spectrum, but the value obtained from the assignment to the 0−1 and 0−2 vibrational bands is closer. In addition, we refer to recent results on the carotenoid spheroidene, where the S_1 energy calculated from the $S_1 \rightarrow S_2$ transient absorption was found to be about 600 cm^{-1} lower as compared to fluorescence measurements.[31] On the basis of these results, we assign the bands observed in the $S_1 \rightarrow S_2$ transient absorption spectrum to the 0−1 and 0−2 vibrational transitions, locating the S_1 energy at 16 100 ± 200 cm^{-1} in *n*-hexane and 16 100 ± 500 cm^{-1} in methanol.

The most striking difference of the peridinin lowest singlet excited state properties in nonpolar and polar solvents is seen in the near-IR transient absorption spectra (Figure 6), where peridinin in methanol exhibits a broad SE band in the 720−1200 nm spectral region 1 ps after excitation, while in *n*-hexane only weak ESA bands can be seen. From the fluorescence spectra (Figure 3) we know that there is substantial fluorescence from the S_1 state in the spectral region 720−850 nm and further

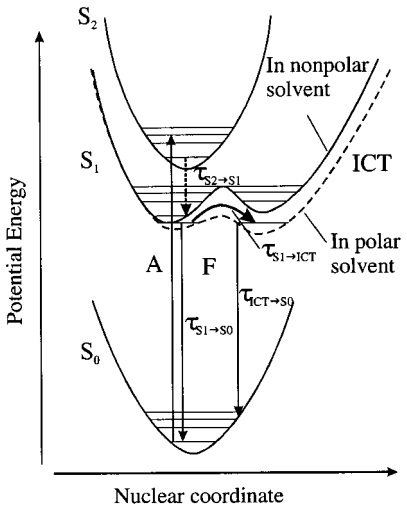

Figure 9. Potential energy surface diagram showing the ground, first, and second singlet excited states of peridinin in nonpolar and polar solvent environment. The S_1 state is strongly coupled with the ICT state. In nonpolar solvents, the barrier between the S_1 and ICT states is high and therefore the ICT state is not populated. In polar solvents, i.e., methanol, the polarity-affected barrier is diminished as the ICT state shifts to lower energy, therefore becoming populated. The transitions and corresponding time constants are shown for the peridinin in polar solvent.

to the red side in both solvents. This implies that in the case of peridinin in *n*-hexane the ESA completely cancels SE and in some regions is even stronger than the SE. The difference between transient absorption spectra of peridinin in methanol and *n*-hexane can be explained by the stronger emission in the red wing of the S_1 fluorescence of peridinin in methanol as compared to *n*-hexane (Figure 3). The characteristic formation time of the SE band of peridinin in methanol can be obtained from the kinetics measured in the spectral range of 600−1800 nm. The results of multiexponential fitting are summarized in Table 2. In the spectral region 600−1500 nm (this spectral interval includes the entire SE band) a component of 1.2 ± 0.3 ps is required to obtain a satisfactory fit. This ∼1 ps time constant corresponds to the appearance of the SE band in the IR region and also characterizes the spectral evolution in the visible region. Fluorescence upconversion experiments in the 727−827 nm region (Figure 8) also show a clear ∼1 ps rise in methanol, confirming the assignment of the negative band (720−1200 nm) observed in the IR transient absorption spectrum of peridinin in methanol to a stimulated emission from a new lower energy state. Moreover, a decay component of 10 ± 1.5 ps is present at all measured wavelengths. Below we will introduce a kinetic model to assign the origin of these time constants. As mentioned in the Results, the fits of the peridinin transient absorption kinetics in *n*-hexane yield a slow decay of 160 ± 15 ps, together with a very fast component of less than 0.2 ps in the majority of traces.

Previous results[15] were interpreted in terms of a kinetic model where the observed decrease of the S_1 lifetimes of peridinin in polar solvents is due to a quenching of the S_1 state by the CT state. With the new findings presented here we can extend this model according to Figure 9 and assign time constants for the relaxation processes involving the CT state. We will call the singlet state with charge-transfer character an intramolecular charge-transfer (ICT) state to avoid confusion with the CT states, from which a charge transfer from the molecule indeed occurs.

To simulate the dynamics of peridinin in methanol, we utilize equations for the population dynamics. Here $[S_0]$, $[S_1]$, $[S_2]$,

$$[S_2] \xrightarrow{k_1} [S_1] \xrightarrow{k_2} [ICT] \xrightarrow{k_3} [S_0] \qquad (1)$$
$$\qquad\qquad\qquad\qquad\qquad\quad k_4$$

and [ICT] are the populations of carotenoid molecules in corresponding levels and $k_1 = 1/\tau_{S_2\rightarrow S_1}$, $k_2 = 1/\tau_{S_1\rightarrow ICT}$, $k_3 = 1/\tau_{ICT\rightarrow S_0}$, and $k_4 = 1/\tau_{S_1\rightarrow S_0}$ are the rate constants. The time constants $\tau_{S_2\rightarrow S_1}$, $\tau_{S_1\rightarrow ICT}$, $\tau_{ICT\rightarrow S_0}$, and $\tau_{S_1\rightarrow S_0}$ are defined in Figure 9. Then the population dynamics of the S_1 and ICT states are described by the equations

$$[S_1] = \frac{Ck_1}{k_2 + k_4 - k_1}(e^{-k_1 t} - e^{-(k_2+k_4)t}) \qquad (2a)$$

$$[ICT] = Ck_1k_2\left\{\frac{e^{-k_1 t}}{(k_2 + k_4 - k_1)(k_3 - k_1)} + \frac{e^{-(k_2+k_4)t}}{(k_1 - k_2 - k_4)(k_3 - k_2 - k_4)} + \frac{e^{-k_3 t}}{(k_1 - k_3)(k_2 + k_4 - k_3)}\right\} \qquad (2b)$$

In these simplified equations it is assumed that the S_2 state is populated instantaneously during excitation and the constant C is the initial S_2 state population after excitation.

On the basis of the experimental results presented here, it is possible to assign the 1 ps component to the time constant $\tau_{S_1\rightarrow ICT}$, characterizing the formation of the ICT state and the 10 ps component to the lifetime of this lowest ICT state ($\tau_{ICT\rightarrow S_0}$). This model fits well to the kinetics measured around 1000 nm, where the signal from the ICT state dominates. However, there are some evident problems with this simple model. First, it cannot explain the fact that the lifetime is independent of the probing wavelength. In both the visible and IR regions, one would expect to find wavelengths corresponding to the ESA from the S_1 state and thus kinetics with 1 ps decay as a dominating time constant. In particular, the decays of the near-infrared $S_1 \rightarrow S_2$ transient absorption spectrum with an ∼10 ps time constant suggest that it is the S_1 state that is characterized by the 10 ps lifetime. Another problem with this relaxation scheme is the small shift of the fluorescence spectrum between methanol and *n*-hexane. From the spectral dynamics observed in the visible spectral region ($S_1 \rightarrow S_n$ and ICT $\rightarrow S_n$ transitions) we can roughly estimate the difference between the S_1 and ICT state to be about 1300 cm^{-1}. The model with a 1 ps time constant for the transfer from the S_1 to the ICT state would require a shift of the fluorescence spectrum to lower energies of about 1300 cm^{-1} as the population from the S_1 state is quickly transferred to the lower-lying emissive state with charge-transfer character. As can be seen from Figure 3, only a small shift of ∼300 cm^{-1} of the maximum is observed, and the fluorescence spectrum of peridinin in methanol demonstrates a broadening rather than a shift.

To solve the apparent contradictions in the model described above, we propose a different kinetic scheme, where the ICT state in methanol relaxes to the ground state with an ∼1 ps time constant ($\tau_{ICT\rightarrow S_0}$), thus the final step in the relaxation process is significantly faster than the $S_1 \rightarrow$ ICT transfer characterized here by an ∼10 ps time constant ($\tau_{S_1\rightarrow ICT}$). In fact, both interpretations (models) are mathematically acceptable at least for dynamics in the spectral region 470−1300 nm; they provide the same shape of kinetic traces, only with different relative amplitudes. However, our interpretation is more consistent with all the data and leads to the population dynamics

of the studied system, which are totally different. In the proposed model the transfer to the ICT state exhibits the strong solvent dependence. Such a solvent dependence of this step can be explained by a solvent-controlled coupling between the S_1 and ICT states, which can be described as a barrier between their corresponding potential energy surfaces. A model with a barrier between the S_1 and ICT states was already indicated for peridinin,[16] but the explanation of the solvent-dependent S_1 lifetimes did not involve the barrier. A model with solvent-dependent barrier has been also proposed to explain dynamics of the twisted intermolecular charge-transfer (TICT) state in the DMABN dye:[32,33] an increase of polarity leads to a more stabilized TICT state having lower energy than in a nonpolar solvent. Since the barrier is the energy difference between the lowest point of the potential energy surface of the "initial" state and the crossing point of the two potential surfaces, the barrier decreases with increasing polarity (Figure 9).

Applying this barrier model to the peridinin S_1 dynamics in the nonpolar solvent *n*-hexane, the coupling between the S_1 and ICT state is so small (barrier is too high) that the ICT state is never populated and we can observe only the S_1 state dynamics. The lifetime of 160 ps of the S_1 state corresponds to the relaxation of the S_1 state directly to the S_0 ground state. Comparing the energy gap between the S_0 and the S_1 states with previous results[12] using the energy gap law,[34] the value of 16 700 cm^{-1} corresponds in the order of magnitude to the observed 160 ps lifetime. Thus, the fluorescence spectrum of peridinin in *n*-hexane reflects merely the emission from the S_1 state. This is the reason we do not see any SE band around 1000 nm in the transient absorption spectrum of peridinin in *n*-hexane, because such emission is characteristic of the ICT state (see below). The dynamic behavior of peridinin in *n*-hexane is generally very similar to that observed for other carotenoids, for which no solvent dependence of the S_1 lifetime was observed.

Transferring peridinin to solvents with higher polarity leads to an increase of the coupling between the S_1 and the ICT states, facilitating transfer of the S_1 population to the lower-lying ICT state. This results in a notable decrease of the fluorescence quantum yield, because the emissive S_1 state is now quenched by the ICT state. In the very polar solvent methanol used in this study, the fluorescence spectrum actually consists of two overlapping bands corresponding to emissions from the S_1 state and from the ICT state. The ICT state emission is shifted to lower energies. Because of the short lifetime of 1 ps compared to the S_1 lifetime of 10 ps, the ICT state is always poorly populated, leading to a broadening rather than to a shift of the fluorescence spectrum at the low-energy side. Emission from the ICT state is readily observed as the SE band in the transient absorption spectrum shown in Figure 6. The high-energy part of the fluorescence spectrum corresponds to the emission from the S_1 state. This is well supported by the fluorescence upconversion experiments summarized in Table 3. Detecting the up-converted signal close to the maximum of the fluorescence spectrum (727 nm), it exhibits only 16% of the 1 ps rise, while the rest of the rise is instantaneous. Furthermore, the amplitude of the 1 ps rise component increases with detection wavelength, comprising more than 40% at 827 nm. Since the S_1 state is populated via internal relaxation from the initially excited S_2 state and since this relaxation is known to occur in ~60 fs[30] (beyond the time resolution of the present experimental setup), the emission from the S_1 state will demonstrate an instantaneous rise. Therefore, the observed behavior agrees well with the idea of two overlapping emission bands corresponding to the emission from the S_1 and ICT states. It is important to note that, since we assume that the S_1 state is depopulated via two different channels (to the ground state and to the ICT state), the time constant $\tau_3 = 10$ ps extracted from the kinetic measurements is $1/\tau_3 = 1/\tau_{S_1 \rightarrow ICT} + 1/\tau_{S_1 \rightarrow S_0}$ according to Figure 9. Assuming that the $S_1 \rightarrow S_0$ depopulation channel is characterized by the same time constant of about 160 ps for all solvents, we can readily calculate the transfer time $\tau_{S_1 \rightarrow ICT}$ of the $S_1 \rightarrow$ ICT channel (Table 1): 11 ps for methanol, 81 ps for 2-propanol, and 148 ps for tetrahydrofuran. For the nonpolar solvent *n*-hexane, $\tau_{S_1 \rightarrow ICT}$ is by definition infinite and the ICT state is never populated.

The model with a polarity-controlled barrier between the S_1 and the ICT states suggested here can be applied to explain also the dynamic behavior of the S_1 states of other carotenoids presented by Frank et al.[16] A similar behavior as found in peridinin was also observed for fucoxanthin and uriolide acetate. For these two carotenoids, however, the solvent polarity dependence of the S_1 lifetime was not so dramatic as in the case of peridinin and the solvent polarity necessary to decrease the S_1 lifetime was found to be higher. Because the S_1 lifetimes of both fucoxanthin and uriolide acetate are shorter in nonpolar solvent than in the case of peridinin (70 ps for both carotenoids), to allow population of the ICT state, the barrier between the S_1 and ICT states must be lower to compete with direct $S_1 \rightarrow S_0$ depopulation. Thus, the solvent polarity at which the S_1 lifetime dependence is obvious must be higher, which is in perfect agreement with results presented in ref 16. The same explanation holds for the carotenoid spheroidenone. This carotenoid exhibits a solvent effect in the S_2 state similar to that observed for peridinin, fucoxanthin, and uriolide acetate: the absorption spectrum is broadened and the vibrational structure is lost as the solvent polarity increases. The S_1 lifetime, however, is unaffected by solvent polarity and remains at 6 ps for all solvents.[16] Such a behavior is not surprising according to the model presented here, since the barrier is probably not low enough to compete with the 6 ps S_1 lifetime even in the most polar solvent used.

Despite this apparent success of the solvent polarity-controlled barrier in explaining experimental observations shown in both this and previous work,[16] we cannot give an unambiguous assignment of the origin of the ICT state observed in various carotenoids. The study by Frank et al.[16] showed that the presence of a carbonyl group in conjugation with the carbon π-electron system is necessary, while neither the allene moiety nor the lactone ring present in peridinin is required for the observed solvent sensitivity, although these groups seem to increase the effect. Another support for the importance of the C═O group is the recent study of apocarotenoids by He et al.[21] They showed that the presence of a terminal CHO group leads to a similar lifetime dependence on solvent polarity, as observed for peridinin and related carotenoids. Thus, the presence of the ICT state in the energy level manifold stems most likely from the interaction of these groups with solvent molecules. In general, the presence of a highly polar emissive ICT state in an excited states manifold is usually characterized by a significant shift of the fluorescence spectrum as polarity of the solvent increases.[35−37] No such behavior was observed here, but the lack of the solvent-dependent Stokes shift was explained by a kinetic scheme in which the final relaxation step is much faster than the transfer of the population to the ICT state. This fact, together with the quite broad fluorescence spectra of carotenoids, fits well to the model incorporating the ICT state. However, we are not able to determine whether the observed ICT state is without torsional

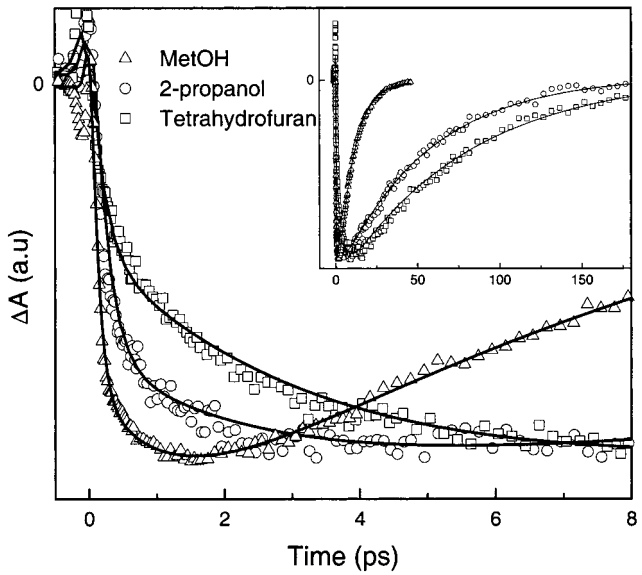

Figure 10. Kinetics of the SE band probed at 975 nm of peridinin in methanol (triangles), 2-propanol (circles), and tetrahydrofuran (squares). In the main picture the first 8 ps of the traces and in the inset the whole decay traces are shown. The solid lines represent multiexponential fits of the data. The amplitudes of traces are normalized to the maximum of the signal. Peridinin was excited at 490 nm.

changes or if a twisting of the carotenoid molecule takes place, forming a TICT state. The barrier model suggested here has been used successfully to explain the behavior of the TICT state,[32,33] but it is worth noting that features similar to those discussed here were observed in the transient absorption spectrum of certain types of push−pull polyenes and ascribed to an excited state reaction, leading to formation of the ICT state.[38]

Another intriguing feature of the model is the very short lifetime of the ICT state: it relaxes to the ground state with a lifetime of 1 ps in methanol. From the shift of the transient absorption spectrum in the visible region (Figure 5), the position of the ICT state can be approximately estimated to be about 1300 cm^{-1} below the S_1 state. Such an assumption puts the energy of the ICT state at approximately 15 000 cm^{-1}, which is obviously too high to explain the 1 ps lifetime based just on the energy gap law and energy separation between the ICT state and bottom of the S_0 state. On the other hand, it is obvious from Table 2 that the rise component characterized by the ∼1 ps time constant and originating from emission from the ICT state extends down to 7100 cm^{-1}, suggesting that the potential surface of the ICT state is rather shallow. In such a case the relaxation from the ICT state to the ground state will occur at a position on the ground state potential surface far away from the minimum, where the energy gap is actually smaller and therefore the relaxation to the ground state faster.

To obtain more information about the ICT state lifetime, we measured the rise of the stimulated emission band at 980 nm for two solvents with medium polarity, 2-propanol and tetrahydrofuran. The results shown in Figure 10 clearly demonstrate the solvent dependence of the ICT state lifetime: going from the most polar solvent methanol to the solvents with medium polarity, the ICT state lifetimes are 1 ps (methanol), 2.5 ps (2-propanol), and 3.5 ps (tetrahydrofuran). Thus, not only is the coupling between the S_1 and ICT states controlled by solvent polarity but also the relaxation from the ICT state to the ground state exhibits solvent polarity dependence. According to Figure 9, such behavior is not surprising, because an increase of stabilization of the ICT state induced by solvent polarity leads to a shift of this state to lower energies. Thus, for the less polar solvents 2-propanol and tetrahydrofuran the energy gap between the ground state S_0 and the ICT state will be bigger than that for methanol, resulting in a longer lifetime of the ICT state. However, to fully explain the excited state dynamics of peridinin, more detailed experiments including both temperature and viscosity dependence along with studies of dynamical behavior of other carotenoids are certainly needed. Furthermore, calculations of the properties of the peridinin lowest singlet excited states would be most helpful.

An important issue is the role that the excited state dynamics of peridinin plays in the PCP complex. It is known that the PCP complex exhibits an extremely high efficiency of carotenoid−chlorophyll energy transfer via the peridinin S_1 state.[14,18] This type of S_1 pathway is confined to a restricted group of eukaryotic algae utilizing oxygenated carotenoids such as fucoxanthin, in addition to peridinin, as principle light-harvesting pigments. The three-dimensional structure of the PCP complex[13] reveals that peridinin resides in a somewhat polar environment created by polar hydrogen bonding residues in addition to a number of water molecules, suggesting that the ICT state could be at least partially populated and therefore play some role in excitation energy flow. Direct measurements of excited state dynamics of peridinin in the protein environment is needed to improve our understanding of the role of the ICT state in the light-harvesting process in the PCP complex.

Acknowledgment. We thank Alexander Tarnovsky, Eva Åkesson, Torbjörn Pascher, Yuri Zaushitsin, Jennifer L. Herek, Frank P. Sharples, and Harry A. Frank for their assistance during the experiments and valuable discussion. This work was supported by the Swedish Natural Science Research Council, the Knut and Alice Wallenberg Foundation, the Crafoord Foundation and the Australian Research Council (A00000264).

References and Notes

(1) Frank, H. A.; Cogdell, R. J. *Photochem. Photobiol.* **1996**, *63*, 257.
(2) Demmig-Adams, B.; Adams, W. W. *Trends Plant Sci.* **1996**, *1*, 21.
(3) Edge, R.; McGarvey, D. J.; Truscott, T. G. *J. Photochem. Photobiol. B* **1997**, *41*, 189.
(4) Christensen, R. L. In *Photochemistry of Carotenoids*; Frank, H. A., Young, A. J., Britton, G., Cogdell, R. J., Eds.; Kluwer Academic Publisher: Dodrecht, The Netherlands, 1999.
(5) Christensen, R. L.; Goyette, M.; Gallagher, L.; Duncan, J.; DeCoster, B.; Lugtenburg, J.; Jansen, F. J.; van der Hoef, I. *J. Phys. Chem. A* **1999**, *103*, 2399.
(6) Schulten, K.; Karplus, M. *Chem. Phys. Lett.* **1972**, *14*, 305.
(7) Hudson, B. S.; Kohler, B. E. *Chem. Phys. Lett.* **1972**, *14*, 299.
(8) Ricci, M.; Bradforth, S. E.; Jimenez, R.; Fleming, G. R. *Chem. Phys. Lett.* **1996**, *259*, 381.
(9) Mimuro, M.; Akimoto, S.; Takaichi, S.; Yamazaki, I. *J. Am. Chem. Soc.* **1997**, *119*, 1452.
(10) Macpherson, A.; Gillbro, T. *J. Phys. Chem. A* **1998**, *102*, 5049.
(11) Nagae, H.; Kuki, M.; Zhang, J.-P.; Sashima, T.; Mukai, Y.; Koyama, Y. *J. Phys. Chem. A* **2000**, *104*, 4155.
(12) Chynwat, V.; Frank, H. A. *Chem. Phys.* **1995**, *194*, 237.
(13) Hofmann, E.; Wrench, P.; Sharples, F. P.; Hiller, R. G.; Welte, W.; Diederichs, K. *Science* **1996**, *272*, 1788.
(14) Bautista, J. A.; Hiller, R, G.; Sharples, F. P.; Gosztola, D.; Wasielewski, M.; Frank, H. A. *J. Phys. Chem. A* **1999**, *103*, 2267.
(15) Bautista, J. A.; Connors, R. E.; Raju, B. B.; Hiller, R. G.; Sharples, F. P.; Gosztola, D.; Wasielewski, M. R.; Frank, H. A. *J. Phys. Chem. B* **1999**, *103*, 8751.
(16) Frank, H. A.; Bautista, J. A.; Josue, J.; Pendon, Z.; Hiller, R. G.; Sharples, F. P.; Gosztola, D.; Wasielewski, M. R. *J. Phys. Chem. B* **2000**, *104*, 4569.
(17) Carbonera, D.; Giacometti, G.; Segre, U.; Hofmann, E.; Hiller, R. G. *J. Phys. Chem. B* **1999**, *103*, 6349.
(18) Kleima, F. J.; Wendling, M.; Hofman, E.; Peterman, E. J. G.; van Grondelle, R.; van Amerongen, H. *Biochemistry* **2000**, *39*, 5184.

(19) Mimuro, M.; Nagashima, M.; Takaichi, S.; Nishimura, Y.; Yamazaki, I.; Katoh, T. *Biochim. Biophys. Acta* **1992**, *1098*, 271.
(20) Akimoto, S.; Takaichi, S.; Ogata, T.; Nishimura, Y.; Yamazaki, I.; Mimuro, M. *Chem. Phys. Lett.* **1996**, *260*, 147.
(21) He, Z.; Gosztola, D.; Deng, Y.; Gao, G.; Wasielewski, M. R.; Kispert, L. D. *J. Phys. Chem. B* **2000**, *104*, 6668.
(22) Zhang, J.-P.; Fujii, R.; Qian, P.; Inaba, T.; Mizaguchi, T.; Koyama, Y.; Onaka, K.; Watanabe, Y.; Nagae, H. *J. Phys. Chem. B* **2000**, *104*, 3683.
(23) Krueger, B. P.; Scholes, G. D.; Jimenez, R.; Fleming, G. R. *J. Phys. Chem. B* **1998**, *102*, 2284.
(24) Connelly, J. P.; Muller, M. G.; Bassi, R.; Croce, R.; Holzwarth, A. *Biochemistry* **1997**, *36*, 281.
(25) Gradinaru, C.; van Stokkum, I. H. M.; Pascal, A. A.; van Grondelle, R.; van Amerongen, H. *J. Phys. Chem B* **2000**, *104*, 9330.
(26) Polívka, T.; Herek, J. L.; Zigmantas, D.; Åkerlund, H.-E.; Sundström, V. *Proc. Natl. Acad. Sci. U.S.A.* **1999**, *96*, 4914.
(27) Martinson, T. A.; Plumley, G. F. *Anal. Biochem.* **1995,** *228*, 123.
(28) Shan, J. *IEEE S. Quantum Electron.* **1988**, *24*, 276.
(29) Macpherson, A. N.; Hiller, R. G.; Hofmann, E.; Gillbro, T. Results presented at the Workshop "Interactions between Chlorophylls and Carotenoids in Photosynthesis" in Antalya, Turkey, 1999.
(30) Yartsev, A.; Zaushitsin, Y.; Zigmantas, D.; Polívka, T.; Sundström V. Work in progress.
(31) Polívka, T.; Zigmantas, D.; Frank, H. A.; Bautista, J. A.; Herek, J. L.; Koyama, Y.; Fujii, R.; Sundström, V. *J. Phys. Chem. B* **2001**, *105*, 1072.
(32) Hicks, J. M.; Vandersall, M. T.; Babarogic, Z.; Eisenthal, K. B. *Chem. Phys. Lett.* **1985**, *116*, 18.
(33) Hicks, J. M.; Vandersall, M. T.; Sitzmann, E. V.; Eisenthal, K. B. *Chem. Phys. Lett.* **1987**, *135*, 413.
(34) Engelman, R.; Jortner, J. *J. Mol. Phys.* **1970**, *18*, 145.
(35) Bhattacharyya, K.; Chowdhury, M. *Chem. Rev.* **1993**, *93*, 507.
(36) Catalan, J.; Diaz, C.; Lopez, V.; Perez, P.; Claramunt, R. M. *J. Phys. Chem.* **1996**, *100*, 18392.
(37) Cornelissen-Gude, C.; Rettig, W. *J. Phys. Chem. A* **1998**, *102*, 7754.
(38) Plaza, P.; Laage, D.; Martin, M. M.; Alain, V.; Blanchard-Desce, M.; Thompson, W. H.; Hynes, J. T. *J. Phys. Chem. A* **2000**, *104*, 2396.